Biofabrication

International Society for Biofabrication

NOTE

Studies of 3D directed cell migration enabled by direct laser writing of curved wave topography

Biofabrication

RECEIVED
11 January 2019

ACCEPTED FOR PUBLICATION
5 February 2019

PUBLISHED
25 February 2019

NOTE

Studies of 3D directed cell migration enabled by direct laser writing of curved wave topography

Daniel Cheng[1,3], **Rachael K Jayne**[2,3], **Alessio Tamborini**[1], **Jeroen Eyckmans**[1,4], **Alice E White**[2,4] and **Christopher S Chen**[1,4]

[1] Department of Biomedical Engineering, Boston University, Boston, MA 02215, United States of America
[2] Department of Mechanical Engineering, Boston University, Boston, MA 02215, United States of America
[3] These authors contributed equally to this work.
[4] Authors to whom any correspondence should be addressed.

E-mail: eyckmans@bu.edu, aew1@bu.edu and chencs@bu.edu

Keywords: direct laser writing (DLW), directional cell migration, topography, Rac1, contact guidance

Supplementary material for this article is available online

Abstract

Cell migration, critical to numerous biological processes, can be guided by surface topography. Studying the effects of topography on cell migration is valuable for enhancing our understanding of directional cell migration and for functionally engineering cell behavior. However, fabrication limitations constrain topography studies to geometries that may not adequately mimic physiological environments. Direct Laser Writing (DLW) provides the necessary 3D flexibility and control to create well-defined waveforms with curvature and length scales that are similar to those found in physiological settings, such as the luminal walls of blood vessels that endothelial cells migrate along. We find that endothelial cells migrate fastest along square waves, intermediate along triangular waves, and slowest along sine waves and that directional cell migration on sine waves decreases as sinusoid wavelength increases. Interestingly, inhibition of Rac1 decreases directional migration on sine wave topographies but not on flat surfaces with micropatterned lines, suggesting that cells may utilize different molecular pathways to sense curved topographies. Our study demonstrates that DLW can be employed to investigate the effects and mechanisms of topography on cell migration by fabricating a wide array of physiologically-relevant surfaces with curvatures that are challenging to fabricate using conventional manufacturing techniques.

1. Introduction

Cell migration plays a central role in a large variety of biological processes including early embryonic development, immune cell trafficking and surveillance, angiogenesis and blood vessel remodeling, cancer metastasis, and tissue repair [1–3]. When cells migrate, they typically move over and across extracellular matrix (ECM), the polymerized fibrous scaffolds that provide the physical structure of our bodies. Interestingly, the structural organization of the ECM influences how cells adhere and migrate. To study these processes in a more controlled setting, researchers generated surfaces patterned with aligned ridges, where it was observed that cells preferentially orient and migrate parallel to the ridges, a phenomenon termed contact guidance [4–7]. Modulating cell migration speed and direction using topography could be valuable for designing biomedical devices where controlled cell repopulation is critical, such as in vascular stents, where an endothelial cell monolayer is necessary for proper vascular function. A major advantage of using topography as a cellular control mechanism for medical implants is that it is purely physical and does not change the biochemistry of the implant environment [8].

Cells exhibit contact guidance on a wide variety of substrate materials and feature sizes ranging from tens of nanometers to hundreds of microns [9–12]. In general, cells tend to migrate faster on patterned surfaces compared to flat surfaces and migration speed decreases at longer wavelengths [10, 13]. To fabricate these surfaces, researchers have predominantly employed lithography-based approaches to produce square-shaped waveforms on which cells generally elongate less as the square wave wavelength becomes longer

[4, 10, 14]. However, square wave topographies are composed of features such as flat surfaces and sharp right-angle edges that are rarely encountered *in vivo*.

How cells respond to and migrate on curved topographies has not been well studied, primarily due to limitations in the ability to fabricate such curved surfaces. Physiological curvatures are present across a range of length scales such as collagen fibers in the ECM with a diameter of 30–100 nm or the lumen of a blood vessel that can range in diameter from tens to hundreds of microns [15]. Researchers have used methods including spin-coating, hydrogel swelling, or polymer deformation to fabricate curved surface topographies [5, 16–21]. Although these studies show that aligned curved surfaces are able to elicit the contact guidance response, many of the fabrication methods are limited in their ability to produce well-defined curved structures with controllable dimensions. Given the prominence of curved features in native tissues, a deeper understanding of how cells sense and respond to such features is important to further elucidate.

In this study, we examine how endothelial cells migrate on curved topography. Endothelial cells migrate along the curved luminal surfaces of blood vessels where the degree of curvature varies with vessel diameter. Furthermore, vascular grafts or stent implants are common procedures that may require cells to migrate along curved topographies to repopulate and form non-thrombogenic surfaces. To produce these curved topographies, we employed an advanced fabrication technique known as Direct Laser Writing (DLW). DLW offers complete 3D spatial control to produce virtually any user-programmed surface with sub-micron resolution. The excellent 3D spatial control of DLW has made it an increasingly popular tool to study the effects of 3D microenvironments in biology and cell migration [22–24]. We used a commercial DLW system (Nanoscribe Photonic Professional GT) and photoresist (IP-Dip, Nanoscribe GmbH) to generate customizable 3D cell-adhesive surfaces to explore the effects of varying waveform, amplitude, and wavelength on Human Umbilical Vein Endothelial Cell (HUVEC) migration. Endothelial cell migration has previously been studied on square wave topography, but not on curved surfaces resembling the lumen of blood vessels where they reside physiologically [12, 25–28]. We then examined both the effects of curved sine wave surfaces on cell migration and the differences in the molecular regulation of directional migration on topography compared to flat chemically-micropatterned surfaces.

2. Materials and methods

2.1. Structure design and DLW fabrication

DLW-printed structures were programmed using MATLAB with 500 nm *z*-steps and 300 nm steps in the *x*–*y* plane. Structures were designed to have an aligned wave topography spanning an area of $3 \times 3\ mm^2$ and to contain a defined starting location for cells in the center of the pattern. The cell starting location consisted of a 'coliseum-like' circular wall structure, which was designed to confine a single droplet of cells suspended in media. The structure had a diameter of 2 mm, a height of 200 μm, and a wall thickness of 15 μm, (figure 1(A)). All structures contained a center seeding ring for controlled cell seeding. The walls of this ring were designed to have large ovular voids to reduce the structure print volume, which in turn minimizes active print time. Importantly, 50 μm diameter semi-circular arches were inserted in the base of the circular wall to allow cells to migrate out of the central region following attachment. To ensure a uniform substrate material for cell attachment and migration, a flat surface was printed inside the coliseum walls.

Structures were printed using IP-Dip photoresist (Nanoscribe GmbH) with scan speed $10\ cm\ s^{-1}$. The minimum feature sizes, or voxel dimensions for the IP-Dip photoresist with the 25× magnification, 1.4 NA objective used in this study are approximately 500 nm in the *x*–*y* plane and 1.5 μm along the *z* axis. PET substrates (Melinex 561 1000 gauge, Dupont) were used to ensure surface adhesion in aqueous solutions for duration of the testing time and for repeated use in future experiments. The substrate interface was detected only once using the system interface finder for each structure to reduce print time, enhance alignment between stitched parts, and prevent interface finding errors. A solid base was included with the topography structures so that they could be printed ~5 μm into the surface of the substrate, ensuring adhesion across the full 3 mm × 3 mm pattern. Samples were prepared so that several individual patterns were printed onto a single substrate at a time. Final optimized print time for a sample with 7 different topography patterns was approximately 14 h (~2 h per structure). After printing, structures were soaked in PGMEA for 40 min to dissolve any remaining unpolymerized photoresist, then briefly rinsed in NOVEC 7100 (3M) solvent. To ensure complete structure polymerization, all prints were exposed to UV light for 20 s.

2.2. Cell culture and seeding

HUVECs (Lonza) were cultured in EGM-2 media (Lonza) at 37 °C in a humidified 5% CO_2 incubator. Prior to seeding, the surfaces were coated with $50\ \mu g\ ml^{-1}$ of human fibronectin (FisherSci) for 1 h then dried using compressed air. To seed cells, a 2 μl droplet of cells (P5-10) at a concentration of 3.3 million cell ml^{-1} (6600 total cells) in EGM-2 was pipetted into the circular cell seeding ring and allowed to adhere for 30 min at 37 °C in a humidified dish. Surface tension caused the liquid droplet, and therefore the cells, to remain confined within the walls. After 30 min, media was added to the entire dish and cells began to migrate out of the walls through the

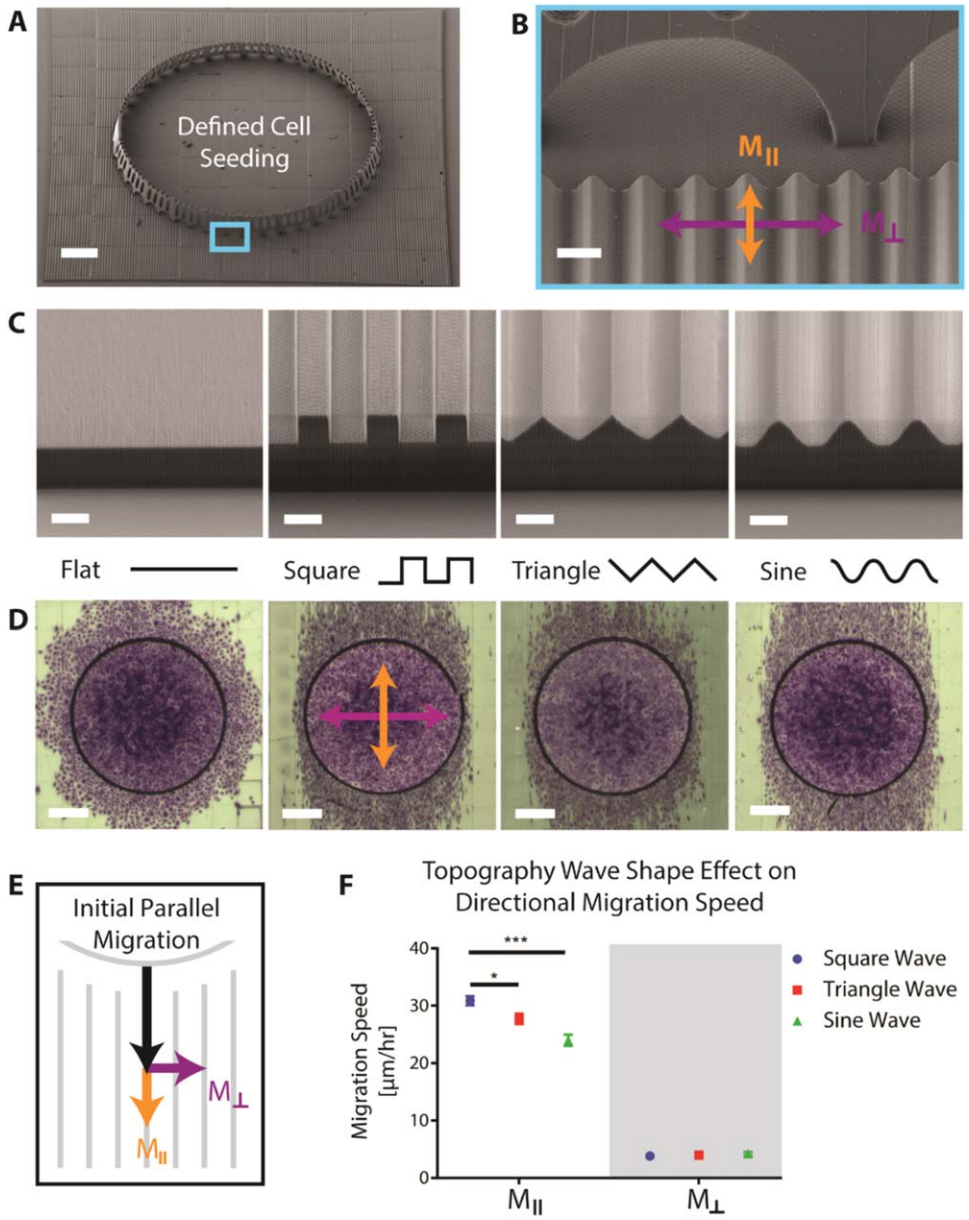

Figure 1. SEM images of (A) a single printed test structure with defined cell seeding location surrounded by aligned square wave topography, scale bar 300 μm, and (B) magnified image of wall arches that allow cells to migrate out following initial seeding, scale bar 20 μm. (C) SEM images of the outer edges of different topography waveforms with 10 μm peak-to-peak amplitude and 20 μm wavelength, scale bar 10 μm. (D) Optical images of the cell migration fronts stained with crystal violet after 24 h on the different topography shapes, scale bar 500 μm. (E) Schematic of cell migration speed broken into its orthogonal components, $M_{||}$ and $M_{\perp}$. (F) Plot showing values of $M_{||}$ and $M_{\perp}$ for different waveform shapes (error bars represent mean $\pm$ SEM). *, **, or *** indicate p-value less than 0.05, 0.01, and 0.001 respectively.

arches. Cell migration fronts were visualized using phase contrast imaging or fixed with 4% paraformaldehyde and stained with crystal violet (FisherSci).

To reuse DLW structures, cells were removed with 0.05% trypsin and substrates were subsequently cleaned using 10% sodium dodecyl sulfate (SDS) solution left on an orbital shaker for at least 24 h followed by multiple washes with 70% ethanol and distilled water.

2.3. Fractional factorial experimental design

We used JMP statistical software package to design a fractional factorial experimental design to screen for significant effects of varying wave shape, amplitude, or wavelength on cell migration. Instead of using a full combinatorial experiment requiring 27 unique patterns, we employed a three-level Taguchi L9 factorial design to collapse the number of patterns to nine while preserving the power to determine the main effect of each parameter on cell migration. We used peak-to-peak amplitudes of 3, 5 or 10 μm, wavelengths of 5, 10, or 20 μm, and three different waveforms: square, triangle, or sinusoid, creating nine combinations with the three set points for each of the three variables. The initial amplitude and wavelength values were taken as the range of dimensions from previous literature that

showed the highest magnitude and most robust effect on cell migration speed from topography [10, 13, 29, 30].

2.4. Single-cell tracking experiments

Cells were recorded using live fluorescence imaging, then cell position tracks were output using the FIJI plugin Trackmate [31, 32]. Cell tracks were filtered to only keep those with good fidelity, as measured through Trackmate's 'quality' filter. A custom MATLAB script was used to analyze the tracks. Average migration speeds were calculated for each cell by calculating the total distance traveled for each hour time interval, then averaging all the time intervals together for each single cell track. To get the final value shown in figures, we averaged values for all cell tracks together over multiple experiments. The angle of migration was calculated for each 1 h interval for each cell and plotted as rose plot histograms.

2.5. Microcontact printing

We used microcontact printing to fabricate coverslips with alternating 10 μm wide parallel lines of cell-adhesive fibronectin and 10 μm wide lines of non cell-adhesive Pluronic F-127. 10 μm width raised lines were molded in PDMS from silicon wafers. 50 mg ml^{-1} fibronectin with 1% Alexa-Fluor-488 conjugated fibronectin was adsorbed to PDMS stamps for 1 h before inverting onto a UV-ozone treated glass coverslip. Coverslips were then treated with 0.2% Pluronic F-127 solution and subsequently washed in PBS. A 2 μl droplet of cells at a concentration of 3.3 million cells ml^{-1} (6600 total cells) in EGM-2 was seeded in a 2 mm diameter PDMS ring. The PDMS ring was removed after 30 min, allowing cells to migrate outward.

2.6. Inhibitor studies

NSC23766 (50 μM), blebbistatin (50 μM), and wortmannin (50 nM) (Tocris Bioscience), were reconstituted and stored in DMSO. Drugs were added in cell media 6 h after initial cell seeding and left for 24 h during imaging.

2.7. Focal adhesion quantification

Cells were stained using anti-paxillin antibody (diluted 1:100, BD Biosciences #610568) and an Alexa-647 goat anti-mouse secondary antibody (1:400, Invitrogen #A21236). Confocal imaging was taken using 0.8 μm slice thickness. Four image slices (total 3.2 μm height) encompassing the peaks of the sine waves were stacked using max projection, processed using FIJI's threshold and watershed functions, then analyzed using the 'analyze particles' function in FIJI. Data from 10 image stacks was averaged, encompassing 20–30 cells total. To quantify focal adhesion length, particles were fitted with an ellipsoid and the major axis length was measured.

2.8. Statistical analysis

The fractional factorial experimental design was set up and analyzed using JMP statistical software package (SAS) using a least squares fit model. Statistical testing and graphing was done using GraphPad Prism software. Single-cell statistics were conducted using two-way ANOVA with a post hoc Dunnett test. Focal adhesion quantification statistics were conducted using students t-test to compare DMSO and NSC conditions.

3. Results

To investigate whether wave shape, amplitude, or wavelength had significant effects on cell migration, we printed patterns with peak-to-peak amplitudes of 3, 5 or 10 μm, wavelengths of 5, 10, or 20 μm, and three different waveforms: square, triangle, or sinusoid (figure 1(B)). The values for wavelength were chosen to be similar in diameter to a spread cell on a flat surface and amplitude values were chosen to span the average values utilized in past studies [9]. Instead of using a full combinatorial experiment requiring 27 unique patterns, we employed a three-level Taguchi L9 factorial design to collapse the number of patterns to nine. This partial factorial experimental design was used to initially screen if there is a significant effect on cell migration when any of the three parameters (amplitude, wavelength, and waveform) are varied. Cells were seeded in the center of each pattern and allowed to migrate for 24 h prior to fixation and staining with crystal violet to visualize the migration front (figure 1(C)). On flat surfaces, cells appeared to migrate out of the walls isotropically, whereas cells on topographies migrated predominantly parallel to the waves independent of the waveform.

While the overall ellipsoidal shape of the migration front on patterned surfaces demonstrated preferential migration, it was not clear how individual cells were behaving and there were no statistically significant differences in the migration speed of the collective cell migration front on the different topographies (figure S1 is available online at stacks.iop.org/BF/11/021001/mmedia). To characterize individual cell migration on the topographies, it was necessary to fluorescently tag the nuclei of the HUVECs by expressing histone H2B-RFP via a lentiviral vector. Single cell migration tracks were recorded using time lapse microscopy. Directional migration of individual cells was quantified by splitting total migration speed into its orthogonal components: parallel ($M_{||}$) or perpendicular ($M_{\perp}$) migration relative to the aligned wave patterns (figure 1(D)). We found that varying wave shape had a significant effect on total migration speed and $M_{||}$, but no significant effect on $M_{\perp}$ (figure 1(E)). Cells migrated fastest on square waves, followed by triangle waves, and lastly sine waves with average speeds of 31.6 ± 1.4, 28.7 ± 1.5, and 25.1 ± 1.7 μm h^{-1}

respectively. We also observed a significant decrease in $M_{\perp}$ as wavelength increased from 3 to 10 μm (table 4.S1). In contrast, varying amplitude did not precipitate significant differences within our tested range for any of the response metrics.

Since the factorial results indicated that topography waveform and wavelength significantly affect migratory behavior of endothelial cells, we decided to study migration as a function of wavelength on the most physiologically relevant yet least-studied waveform, the sine wave. Whereas a number of publications have shown that square wave features with dimensions as small as 35 nm can direct cell migration, the upper limit of feature sizes that a cell will respond to is not well defined, especially for curved topographies [15]. We proceeded to explore the effects of longer wavelength sine wave topographies with a fixed 10 μm peak-to-peak amplitude and wavelengths of 20, 50, 100, or 150 μm (figure 2(A)). It was observed that as wavelength increased, the shape of the cell migration front transitioned from visibly elliptical to a more isotropic migration pattern resembling that of a flat surface (figure 2(B)). These findings were corroborated by single-cell analysis, which showed slower $M_{||}$ and faster $M_{\perp}$ migration speeds as wavelength increased (figures 2(C) and (E)). The trend for $M_{\perp}$ was the opposite of what we observed when wavelength was varied from 3 to 10 μm, indicating that there may be a local mimimum for the perpendicular component of cell migration speed at the 10 μm wavelength. However, since the previous data was part of a fractional factorial screening experiment where wave shape and amplitude were also varied, the data should not be directly compared. Variability of the angle of migration, visualized by rose plot histograms, also increased at longer wavelengths (figure 2(D)). In comparison with flat printed patterns, $M_{||}$ was only significantly faster on the 20 μm wavelength and $M_{\perp}$ was significantly slower than $M_{||}$ across all wavelengths (figure 2(E)). Even though the magnitude of the effect of topography on cell migration decreased at longer wavelengths, cells were still able to sense and respond to sinusoidal topographies with 150 μm wavelength, roughly three to four times the diameter of a single cell. Although there were significant effects of varying wavelength on $M_{||}$ and $M_{\perp}$, there were no differences in total migration speed across the various wavelengths (figure S3).

To quantify the anisotropy of the observed migration, we calculated the anisotropy ratio, defined as $M_{||}/M_{\perp}$. The anisotropy ratio was highest for the 20 μm wavelength (~5) and decreased at longer wavelengths, approaching isotropy (1) (figure 2(F)). Although the anisotropy ratio was lowest for the flat printed patterns, migration was not isotropic. We compared flat patterns printed using DLW with those with a flat spin coated surface and found differences in $M_{||}$ between the two (figures 2(E) and (F)). SEM imaging of the flat printed topographies showed the presence of aligned nanoscale topography formed from incomplete voxel overlap between printed lines (figure S2). These small aligned grooves were approximately 100 nm deep and spaced at the width of one voxel (300 nm) from each other and were enough to significantly increase $M_{||}$ speed on 'flat' printed patterns when compared to the spin coated migration (figure 2(E)). Nonetheless, the topographies of all substrates were printed in the same orientation using the same printing parameters, allowing us to make controlled comparisons within our system framework.

Directional cell migration arises from cell polarization, where cells have a protrusive front and a contractile rear. Some of the molecular pathways involved in cell polarization have previously been revealed by 2D cell migration studies that used microcontact printing to pattern adhesive ligands on flat surfaces [33, 34]. Three major molecular drivers identified in directional migration are non-muscle myosin II (NMMII), which forms contractile actomyosin bundles at the cell rear and locally inhibits protrusion initiation, phosphoinositide 3-kinase (PI3K), which regulates a number of pathways involved in actin cytoskeletal remodeling in cell migration, and Rac1, which locally concentrates actin polymerization and lamellipodial protrusion to the cell front [1, 35]. However, it remains unclear how insights from these 2D migration studies translates to curved topographies, and if the molecular pathways are similar.

To explore whether directional migration induced by topography uses the same molecular mechanisms as those previously described for flat substrates, we added inhibitors of NMMII, PI3K, and Rac1 to cells on the 20 μm wavelength sine waves. Cell migration on these sine waves was compared to the migration of cells treated with the same inhibitors on flat substrates patterned with fibronectin-coated lines. Alternating 10 μm wide lines of cell-adhesive fibronectin and non-adhesive Pluronic were microcontact-printed onto glass (figure 3(A)). The flat lines induced cell elongation and directional migration in the parallel direction analogous to our topographies and similar previous reports (figure 3(B)) [13, 34]. Cell seeding density was kept constant and seeding was confined using PDMS rings to keep conditions as similar as possible to that of cells on the sine waves.

Two out of the three selected inhibitors, NMMII and PI3k, elicited a similar response in both surface types. The NMMII inhibitor blebbistatin decreased $M_{||}$ and $M_{\perp}$ on both sine waves and flat lines (figures 3(C) and (F)). The PI3k inhibitor wortmannin reduced cell elongation and modestly decreased directional cell migration (decreased $M_{||}$, increased $M_{\perp}$) for both the sine waves and flat lines (figures 3(D) and (G)). Interestingly, the Rac1 inhibitor NSC23766 increased directional migration of cells on the flat lines, consistent with previous reports, but had the opposite effect for cells on the sine waves [34]. On flat lines NSC23766 increased $M_{||}$ and decreased $M_{\perp}$, but on sine waves NSC23766

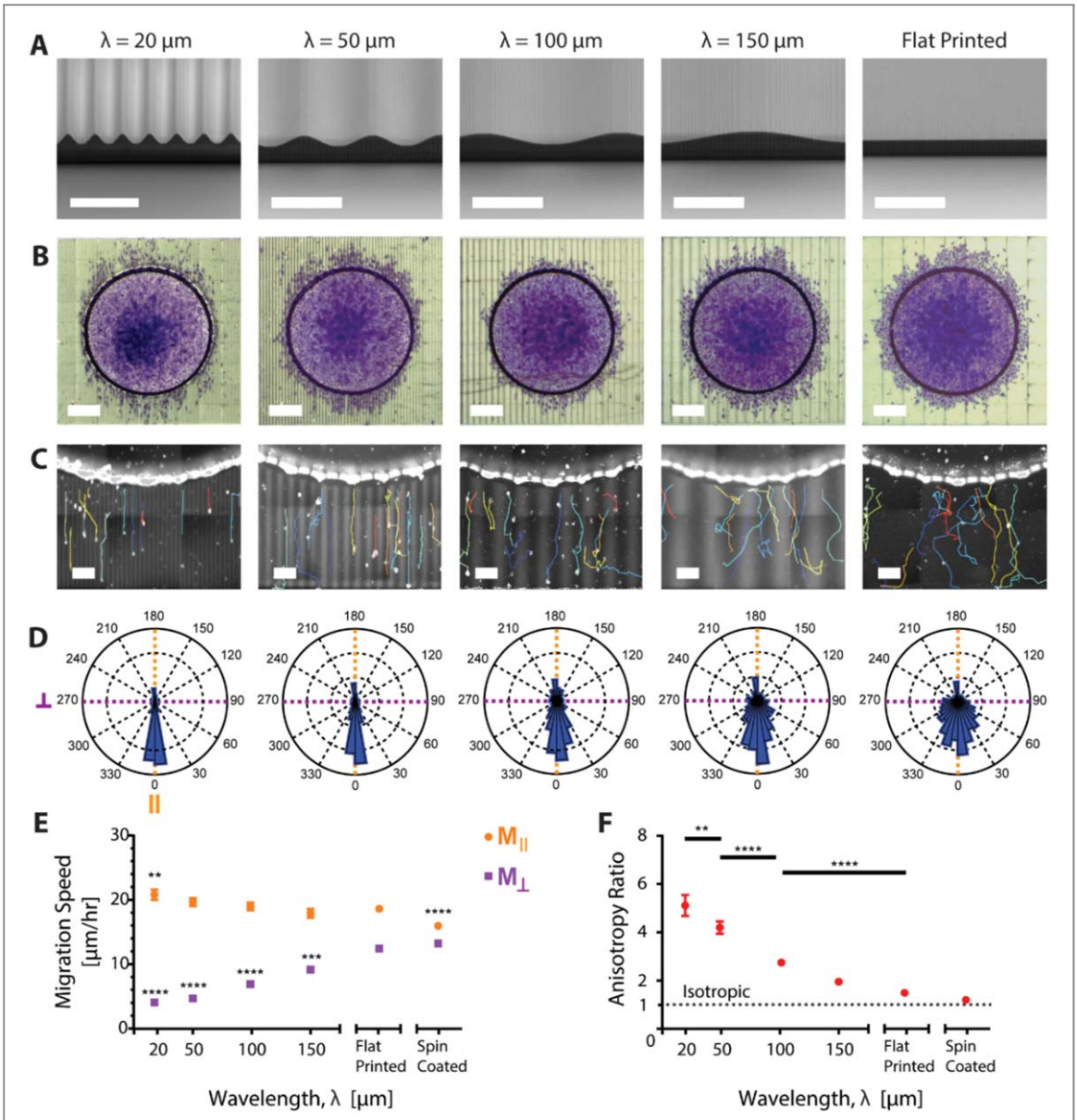

Figure 2. (A) SEM images of sine-wave topography prints with varying wavelength. Scale bar, 50 μm. (B) Optical images of the cell migration front on the varied wavelength (λ) sine waves. Cells were fixed and stained with crystal violet. Scale bar, 300 μm. (C) Representative single cell tracks output from Trackmate overlaid onto an image of H2B-RFP tagged cell nuclei. Printed patterns are autofluorescent and thus visible along with cell nuclei. Higher intensity areas denote the peaks of the sine waves while lower intensity areas denote the troughs. Scale bar, 50 μm. (D) Rose plot histograms of the angle of cell migration over 1 h time intervals for each wavelength. Angle of migration was rotated so that the initial direction of migration out of the walls was in the 0° direction. Each plot shows combined data with $n = 8$. (E) $M_{||}$ (orange) and $M_{\perp}$ (purple) cell migration speed with varying wavelength. * indicates significance as compared to the flat printed condition. (F) Migration speed anisotropy ratio: the ratio of $M_{||}/M_{\perp}$ migration across the various wavelengths. An anisotropy ratio of 1 indicates isotropic migration. *, **, ***, or **** indicate p-value less than 0.05, 0.01, 0.001, and 0.0001 respectively. All error bars represent mean ± SEM.

decreased $M_{||}$ and increased $M_{\perp}$ (figures 3(E) and (H)). These findings suggest that endogenous Rac1 may suppress directional migration on flat surfaces but is in fact important for mediating topography-induced directional migration (figure 3(H)).

To gain a better understanding of the observed Rac1 inhibitor behavior, we examined focal adhesion (FA) formation between treated and untreated cells on both the patterned FN lines and sine wave topographies. One of the hypothesized underlying causes of contact guidance is the regulation of FA area by physical topography, where FA elongation is constrained in the perpendicular direction, leading to proportionally more parallel FAs [36–38]. Results showed that cells on the sine waves had significantly less FA formation when treated with NSC (figure 3(I)). Quantification revealed significantly higher average FA area and length for control versus NSC23766 conditions (figures 3(K) and (L)). In contrast, cells on flat fibronectin lines had the same amount of FA formation in the control and NSC conditions (figures 3(J)–(L)). These results are consistent with a model whereby the enhanced directional migration caused by sine wave topographies may be mediated by a Rac-dependent

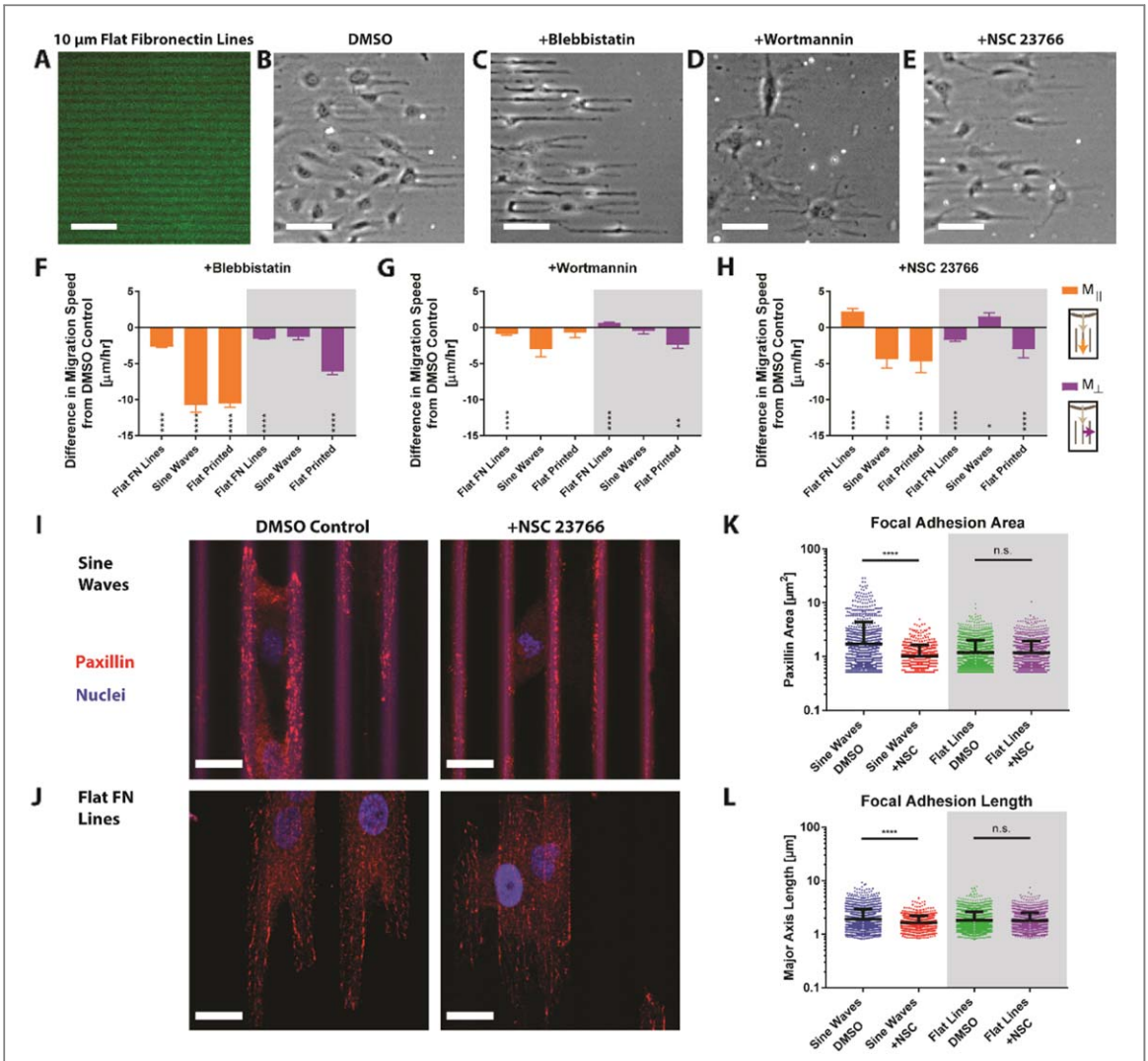

Figure 3. (A) Microcontact-printed flat fluorescent green fibronectin lines of 10 μm width. (B) Cells were seeded in a circle then migrated out along the lines, left to right. Scale bar, 100 μm. (B) DMSO, (C) blebbistatin, (D) wortmannin, or (E) NSC 23766 was added 6 h after seeding. Cell migration on flat fibronectin (FN) lines, sine waves, or flat printed patterns was recorded and compared to the DMSO control for (F) blebbistatin, (G) wortmannin, or (H) NSC (error bars represent mean $\pm$ SEM). (I) Confocal imaging of cells migrating on sine waves stained for paxillin and cell nuclei with either DMSO (left) or NSC (right) added. Scale bar, 20 μm. (J) Cells migrating on flat FN lines stained for paxillin and cell nuclei with either DMSO (left) or NSC (right) added. Scale bar, 20 μm. Quantification of (K) focal adhesion area and (L) focal adhesion length for each condition (error bars represent mean $\pm$ SD). *,**,***, or **** indicate p-value less than 0.05, 0.01, 0.001, and 0.0001 respectively.

increase in FA area and length on the sine waves, leading to increased cell polarization. This model supports previous suggestions that the underlying cause of contact guidance involves regulation of FAs by the physical topography [21, 36, 37, 39].

4. Discussion

This study highlights the importance of studying cell migration on biologically relevant curved topographies. HUVEC migration is different on curved topographies compared to square wave topographies often used for topography studies. Song *et al* have previously used x-ray lithography to fabricate well-defined sinusoidal waves to study T-cell migration and found that cells migrated preferentially within the troughs of the waves, more so on shorter wavelength waves [40]. Although x-ray lithography proves to be an acceptable fabrication method for creating various sine wave features, it may not be ideal for users to produce a new x-ray mask for every new structure they would like to test. DLW is well suited for producing various curved topographies since it can provide the resolution of a photolithography process without having to use a mask. Using DLW-printed curved topographies, we found that endothelial cells had decreased directional migration on sine wave topographies with longer wavelengths. Interestingly, HUVECs continued to exhibit directional migration on sine waves with wavelengths even as long as 150 μm, a length scale significantly longer than the span of individual cells.

While the field has largely presumed that contact guidance by flat adhesive patterns such as parallel lines and by 3D topographic features would occur via a

common mechanism, our results suggest fundamental differences between the two processes, exemplified by an important role for the Rac1 GTPase in topography-induced guidance of cell migration that was opposite to its role in cells on flat adhesive patterns. Analysis of FA area on both flat FN-patterned and sine wave surfaces supports the hypothesis that contact guidance is influenced by the topographic constraints on FA formation. FA proteins mechanically link the cell's actin cytoskeleton to the extracellular environment, and are critical for force transduction that occurs in the cell during migration [41]. As cells spread and elongate parallel to topography, FAs mature, elongate, and align within the cell coordinately with the direction of actin stress fibers, stabilizing cellular forces along the axis of elongation. FA alignment and elongation parallel to the topography may lead to anisotropic force distribution and to cell polarization [11, 21, 37, 42]. The observation that Rac1 inhibition leads to both decreased directional migration and reduced FA length supports the hypothesis that Rac1 is linked to the contact guidance effect, and illuminates a potential pathway by which Rac1 could be important to FA maturation, elongation, alignment on sine wave topography.

5. Conclusion

We report a method of studying cell behavior on curved topographies at biologically relevant length scales. This approach enables rapid iteration through different topographic designs that would otherwise be difficult to fabricate using traditional microfabrication techniques in order to identify how parameters such as waveform, wavelength, and amplitude impact contact guidance of endothelial cells. It remains to be explored whether the findings we observed are dependent on cell type or FN surface coating. DLW has proven to be an excellent tool for producing customizable topographical features suitable for contact guidance studies. Along with the high resolution that DLW offers comes relatively small writing areas, making it difficult to print uniform topography patterns over large surface areas. To address this, we stitched together these writing areas to form structures that can span large regions (up to the area of a 4 inch wafer), but trade-offs included long print times as well as sample tilt complications. Although there are some technical tradeoffs for DLW as a fabrication method, it can be used to produce high resolution structures for a variety of biological studies. It is important to note that although the curved topography structures produced in this study are 3D, cell migration is still significantly constrained to the topographic surface, and more work is needed to study contact guidance in a truly unconstrained 3D environment. Going forward, DLW can be used to systematically study the effect of novel geometries on cell migration and behavior.

Acknowledgments

Daniel Cheng and Rachael Jayne contributed equally to this work. This research was supported in part by the Boston University College of Engineering, the Boston University Photonics Center, the National Science Foundation Graduate Research Fellowship Program (DC), the Clare Boothe Luce Graduate Research Fellowship (RKJ), and by the NSF CELL-MET ERC award no. 1647837.

ORCID iDs

Daniel Cheng https://orcid.org/0000-0003-4464-0061

References

[1] Petrie R J, Doyle A D and Yamada K M 2009 Random versus directionally persistent cell migration *Nat. Rev. Mol. Cell Biol.* **10** 538–49
[2] Friedl P and Wolf K 2003 Tumour-cell invasion and migration: diversity and escape mechanisms *Nat. Rev. Cancer* **3** 362–74
[3] Daley W P and Yamada K M 2013 ECM-modulated cellular dynamics as a driving force for tissue morphogenesis *Curr. Opin. Genet. Dev.* **23** 408–14
[4] Clark P, Connolly P, Curtis A S, Dow J A and Wilkinson C D 1990 Topographical control of cell behaviour: II. Multiple grooved substrata *Development* **108** 635–44
[5] Bettinger C J, Orrick B, Misra A, Langer R and Borenstein J T 2006 Microfabrication of poly (glycerol–sebacate) for contact guidance applications *Biomaterials* **27** 2558–65
[6] Bain J, Plater L, Elliott M, Shpiro N, Hastie C J, Mclauchlan H, Klevernic I, Arthur J S C, Alessi D R and Cohen P 2007 The selectivity of protein kinase inhibitors: a further update *Biochem. J.* **408** 297–315
[7] Den Braber E T, De Ruijter J E, Smits H T J, Ginsel L A, Von Recum A F and Jansen J A 1996 Quantitative analysis of cell proliferation and orientation on substrata with uniform parallel surface micro-grooves *Biomaterials* **17** 1093–9
[8] Miyoshi H, Adachi T, Ju J, Lee S M, Cho D J, Ko J S, Uchida G and Yamagata Y 2012 Characteristics of motility-based filtering of adherent cells on microgrooved surfaces *Biomaterials* **33** 395–401
[9] Nikkhah M, Edalat F, Manoucheri S and Khademhosseini A 2012 Engineering microscale topographies to control the cell–substrate interface *Biomaterials* **33** 5230–46
[10] Kaiser J-P, Reinmann A and Bruinink A 2006 The effect of topographic characteristics on cell migration velocity *Biomaterials* **27** 5230–41
[11] Teixeira A I, McKie G A, Foley J D, Bertics P J, Nealey P F and Murphy C J 2006 The effect of environmental factors on the response of human corneal epithelial cells to nanoscale substrate topography *Biomaterials* **27** 3945–54
[12] Biela S A, Su Y, Spatz J P and Kemkemer R 2009 Different sensitivity of human endothelial cells, smooth muscle cells and fibroblasts to topography in the nano–micro range *Acta Biomater.* **5** 2460–6
[13] Li S, Bhatia S, Hu Y, Shiu Y, Li Y, Usami S and Chien S 2001 Effects of morphological patterning on endothelial cell migration *Biorheology* **38** 101–8
[14] Lu X and Leng Y 2003 Quantitative analysis of osteoblast behavior on microgrooved hydroxyapatite and titanium substrata *J. Biomed. Mater. Res.* **66A** 677–87

[15] Loesberg W A, te Riet J, van Delft F C M J M, Schön P, Figdor C G, Speller S, van Loon J J W A, Walboomers X F and Jansen J A 2007 The threshold at which substrate nanogroove dimensions may influence fibroblast alignment and adhesion *Biomaterials* **28** 3944–51
[16] Guvendiren M, Yang S and Burdick J A 2009 Swelling-induced surface patterns in hydrogels with gradient crosslinking density *Adv. Funct. Mater.* **19** 3038–45
[17] Yang P, Baker R M, Henderson J H and Mather P T 2013 *In vitro* wrinkle formation via shape memory dynamically aligns adherent cells *Soft Matter* **9** 4705
[18] Lam M T, Sim S, Zhu X and Takayama S 2006 The effect of continuous wavy micropatterns on silicone substrates on the alignment of skeletal muscle myoblasts and myotubes *Biomaterials* **27** 4340–7
[19] Lee J, Chung S, Song H, Kim S and Hong Y 2013 Lateral-crack-free, buckled, inkjet-printed silver electrodes on highly pre-stretched elastomeric substrates *J. Phys. D: Appl. Phys.* **46** 105305
[20] Brau F, Vandeparre H, Sabbah A, Poulard C, Boudaoud A and Damman P 2011 Multiple-length-scale elastic instability mimics parametric resonance of nonlinear oscillators *Nat. Phys.* **7** 56–60
[21] Saito A C, Matsui T S, Ohishi T, Sato M and Deguchi S 2014 Contact guidance of smooth muscle cells is associated with tension-mediated adhesion maturation *Exp. Cell Res.* **327** 1–11
[22] Jeon H, Hidai H, Hwang D J, Healy K E and Grigoropoulos C P 2010 The effect of micronscale anisotropic cross patterns on fibroblast migration *Biomaterials* **31** 4286–95
[23] Tayalia P, Mendonca C R, Baldacchini T, Mooney D J and Mazur E 2008 3D cell-migration studies using two-photon engineered polymer scaffolds *Adv. Mater.* **20** 4494–8
[24] Richter B, Hahn V, Bertels S, Claus T K, Wegener M, Delaittre G, Barner-Kowollik C and Bastmeyer M 2017 Guiding cell attachment in 3D microscaffolds selectively functionalized with two distinct adhesion proteins *Adv. Mater.* **29** 1604342
[25] Franco D, Klingauf M, Bednarzik M, Cecchini M, Kurtcuoglu V, Gobrecht J, Poulikakos D and Ferrari A 2011 Control of initial endothelial spreading by topographic activation of focal adhesion kinase *Soft Matter* **7** 7313
[26] Uttayarat P, Toworfe G K, Dietrich F, Lelkes P I and Composto R J 2005 Topographic guidance of endothelial cells on silicone surfaces with micro- to nanogrooves: orientation of actin filaments and focal adhesions *J. Biomed. Mater. Res.* A **75** 668–80
[27] Franco D, Milde F, Klingauf M, Orsenigo F, Dejana E, Poulikakos D, Cecchini M, Koumoutsakos P, Ferrari A and Kurtcuoglu V 2013 Accelerated endothelial wound healing on microstructured substrates under flow *Biomaterials* **34** 1488–97
[28] Morgan J T, Wood J A, Shah N M, Hughbanks M L, Russell P, Barakat A I and Murphy C J 2012 Integration of basal topographic cues and apical shear stress in vascular endothelial cells *Biomaterials* **33** 4126–35
[29] Kim D-H, Han K, Gupta K, Kwon K W, Suh K-Y and Levchenko A 2009 Mechanosensitivity of fibroblast cell shape and movement to anisotropic substratum topography gradients *Biomaterials* **30** 5433–44
[30] Dalton B A, Walboomers X F, Dziegielewski M, Evans M D M, Taylor S, Jansen J A and Steele J G 2001 Modulation of epithelial tissue and cell migration by microgrooves *J. Biomed. Mater. Res.* **56** 195–207
[31] Tinevez J Y, Perry N, Schindelin J, Hoopes G M, Reynolds G D, Laplantine E, Bednarek S Y, Shorte S L and Eliceiri K W 2017 TrackMate: an open and extensible platform for single-particle tracking *Methods* **115** 80–90
[32] Schindelin J *et al* 2012 Fiji: an open-source platform for biological-image analysis *Nat. Methods* **9** 676–82
[33] Pankov R, Endo Y, Even-Ram S, Araki M, Clark K, Cukierman E, Matsumoto K and Yamada K M 2005 A Rac switch regulates random versus directionally persistent cell migration *J. Cell Biol.* **170** 793–802
[34] Doyle A D, Wang F W, Matsumoto K and Yamada K M 2009 One-dimensional topography underlies three-dimensional fibrillar cell migration *J. Cell Biol.* **184** 481–90
[35] Jiménez C, Portela R A, Mellado M, Rodríguez-Frade J M, Collard J, Serrano A, Martínez-A C, Avila J and Carrera A C 2000 Role of the PI3K regulatory subunit in the control of actin organization and cell migration *J. Cell Biol.* **151** 249–61
[36] Ventre M, Natale C F, Rianna C and Netti P A 2014 Topographic cell instructive patterns to control cell adhesion, polarization and migration *J. R. Soc. Interface* **11** 20140687–20140687
[37] Ray A, Lee O, Win Z, Edwards R M, Alford P W, Kim D H and Provenzano P P 2017 Anisotropic forces from spatially constrained focal adhesions mediate contact guidance directed cell migration *Nat. Commun.* **8** 14923
[38] Kubow K E, Conrad S K and Horwitz A R 2013 Matrix microarchitecture and myosin II determine adhesion in 3D matrices *Curr. Biol.* **23** 1607–19
[39] Ohara P T and Buck R C 1979 Contact guidance *in vitro*. A light, transmission, and scanning electron microscopic study *Exp. Cell Res.* **121** 235–49
[40] Song K H, Park S J, Kim D S and Doh J 2015 Sinusoidal wavy surfaces for curvature-guided migration of Tlymphocytes *Biomaterials* **51** 151–60
[41] Brown M C and Turner C E 2004 Paxillin: adapting to change *Physiol. Rev.* **84** 1315–39
[42] Balaban N Q *et al* 2001 Force and focal adhesion assembly: a close relationship studied using elastic micropatterned substrates *Nat. Cell Biol.* **3** 466–72